



Article

Lift Augmentation at Subsonic Speeds by Lateral Jets for a Hypersonic Aircraft

Haifeng Wang ¹, Jianxia Liu ², Feng Deng ^{1,*}, Guoshu Li ³, Yunguang Ding ³, Qiang Xia ³ and Fan Zhang ³

¹ College of Aerospace Engineering, Nanjing University of Aeronautics and Astronautics, Nanjing 210016, China

² Aerospace Technology Institute of CARDC, Mianyang 621000, China

³ Science and Technology on Space Physics Laboratory, Beijing 100076, China

* Correspondence: fdeng@nuaa.edu.cn

Abstract: This paper presents a numerical investigation on the lift augmentation at subsonic speeds by using lateral jets for a hypersonic aircraft equipped with a waverider-type lifting body, which consists of three main parts. The jet slots were arranged along the side edges of the lifting body to study the effect of lateral blowing on the lift augmentation at a freestream Mach number of 0.3. The numerical results based on solving the Reynolds-averaged Navier–Stokes equation indicate that a well-designed lateral blowing can produce a significant lift rise. Then, further work was carried out to investigate the effects of jet parameters, including the jet location, the blowing strength and the blowing direction on lift augmentation, and to provide insights into the associated flow physics. It was found that blowing on the middle and rear parts of the lifting body achieves the maximum lift augmentation among the chosen configurations. Additionally, it was confirmed that the lift augmentation increases as the jet momentum increases, and blowing in the direction of $\theta_{jet} = -45^\circ$, which means the jet blows slightly towards the lower surface of the lifting body, produces a larger lift rise than other directions. The lift augmentation can be explained by the fact that a well-designed lateral blowing can amplify the effectiveness of the vortices shedding from the side edges of the lifting body, resulting in an increase in the vortex lift.

Keywords: flow control; hypersonic aircraft; lift augmentation; lateral jet; vortex lift



Citation: Wang, H.; Liu, J.; Deng, F.; Li, G.; Ding, Y.; Xia, Q.; Zhang, F. Lift Augmentation at Subsonic Speeds by Lateral Jets for a Hypersonic Aircraft. *Aerospace* **2022**, *9*, 745. <https://doi.org/10.3390/aerospace9120745>

Academic Editors: Roberta Fusaro and Mattia Barbarino

Received: 4 November 2022

Accepted: 21 November 2022

Published: 23 November 2022

Publisher's Note: MDPI stays neutral with regard to jurisdictional claims in published maps and institutional affiliations.



Copyright: © 2022 by the authors. Licensee MDPI, Basel, Switzerland. This article is an open access article distributed under the terms and conditions of the Creative Commons Attribution (CC BY) license (<https://creativecommons.org/licenses/by/4.0/>).

1. Introduction

Being able to take off or land horizontally is highly desirable for a hypersonic aircraft. The aerodynamic shape of a hypersonic aircraft is usually designed as a low aspect ratio lifting body, also known as a waverider, to increase its lift–drag ratio at hypersonic speeds [1,2]. However, a low aspect ratio configuration cannot produce enough lift for a horizontal takeoff or a horizontal landing. Therefore, it is of practical significance to find an effective way to increase the lift of a hypersonic aircraft flying at low speeds.

At low speeds, the lift on an aircraft is traditionally increased by either temporarily changing the aerodynamic shape using the high-lift devices, such as slats or flaps, or permanently adopting an auxiliary lift surface, such as a canard or a strake-wing. Smith [3] has investigated the effects of the camber, the effective chord and the interference between different flaps on the low-speed performance of a civil aircraft. Then, Staelens et al. [4] proposed a belly-flap control method to enhance the lift and the pitching moment of a Blended Wing Body airplane during landing, go-around and takeoff. Hummel and Oelker [5] studied the vortices produced by the canard and the wing, pointing out that the trailing vortices of the canard would merge with the boundary layer on the wing surface and reduce the vortices shedding from the side edges of the wing, thus delaying the flow separation and increasing the maximum lift. Tu [6] investigated the effect of the canard vertical position on the aerodynamic performance, confirming two unsolved problems,

which were the canard stall and the undesirable interference between the canard and the wing, respectively. Luckring [7] compared a strake-wing configuration and a canard-wing configuration, concluding that the former would produce a higher lift due to a favorable interference. Additionally, the high-lift devices were geometrically parameterized and optimized for maximizing the lift by Tian et al. [8]. However, although the conventional approaches can effectively increase the maximum lift of a subsonic aircraft or a supersonic aircraft, they are not suitable for a hypersonic aircraft due to the very low aspect ratio.

Recently, active flow control technologies have been introduced into the next-generation aircraft due to their higher adaptability, lower inertia and shorter delay time in comparison with that of conventional methods. They were mainly used for flow separation suppression [9,10], gust alleviation [11], drag reduction [12], lift augmentation [13], missile control [14–16] and heat protection [17,18]. Among the active flow control methods, jets are especially attractive for improving the performance of a supersonic vehicle, as shown in the study by Dong et al. [19]. Jets have been applied in missile control and aerodynamic heat protection as well. For example, Srivastava [14,15] investigated the interaction between the lateral jets and the external flow around a generic missile body. Jiang et al. [20] applied lateral jets to reduce the drag and enhance the thermal protection of a hypersonic vehicle.

More works aimed to improve the subsonic aerodynamic performances of supersonic air vehicles by using jets. Erickson and Campbel [21] proposed to use the spanwise blowing on the canard-wing to improve the maneuver characteristics of a fighter aircraft, confirming that blowing could delay the vortex breakdown and improve the efficiency of canard control. Liu et al. [22] continued their work and found that both the lift and the stall angle increased as the jet momentum coefficient increased. Satran et al. [23] reported a study on the spanwise blowing on a fighter aircraft, showing that the blowing could provide a significant lift augmentation, as well as an increase in the lateral-directional stability. Hong et al. [24,25] investigated the effects of lateral blowing along the leading edge of a delta wing, concluding that the higher the blowing rate, the greater the forces and the moments attained on the model. In addition to the leading edge, Kamishita et al. [26–28] conducted a number of experimental studies by arranging lateral blowing near the trailing edge of an arrow wing, confirming that the lateral jets were useful for improving the aerodynamic characteristics of the arrow wing at both low and high speeds. In a low-speed wind tunnel, Tadakuma et al. [29] continued Kamishita et al.'s works and found that the lateral jets near the trailing edge of a wing-body configuration could increase the lift over a wide range of angles of attack. Additionally, Muramatsu et al. [30] investigated the effect of blowing direction on delaying the vortex breakdown. Zhang et al. [31] compared four types of nozzle shape, concluding that the elliptical shape had the best performance in terms of lateral control efficiency. Doolabi and Sabour [32] proposed a new arrangement of lateral jets to control the roll moment or the pitch moment of a Finner model over a wide range of speeds.

As mentioned above, most of research focuses on simple wings, such as a delta wing or an arrow wing, designed for flying at supersonic speeds. The effectiveness of lateral jets in improving the low-speed performance of a hypersonic aircraft is still unknown. This work aims to investigate the potential of lateral jets in augmenting the lift of a hypersonic aircraft at subsonic speeds, and to further understand the associated flow physics. The paper is organized as follows. The numerical methods are first presented, followed by a validation based on the experimental data and a grid convergence study. Then, the effects of jet parameters, including the jet location, the blowing strength and the blowing direction on lift augmentation, are investigated respectively, followed by the conclusions.

2. Numerical Methods

2.1. Governing Equations

By assuming a steady compressible flow, the chosen governing equations were the Reynolds-averaged Navier–Stokes equations, solved by Ansys Fluent 19.4 and defined as follows

$$\frac{\partial}{\partial t} \iiint W d\Omega + \iint (F_c - F_v) dS = 0 \quad (1)$$

where W is the conserved variables, F_c is the convective flux terms and F_v is the viscous flux terms. The variables and the fluxes are

$$W = \begin{pmatrix} \rho \\ \rho v_x \\ \rho v_y \\ \rho v_z \\ E \end{pmatrix}, F_c = \begin{pmatrix} \rho V \\ \rho V v_x + p \hat{i} \\ \rho V v_y + p \hat{j} \\ \rho V v_z + p \hat{k} \\ (E + p)V \end{pmatrix}, F_v = \begin{pmatrix} 0 \\ \tau_{xi} \\ \tau_{yi} \\ \tau_{zi} \\ \tau_{ij} v_j - q \end{pmatrix} \quad (2)$$

where ρ , p , V and E are the air density, the air pressure, the velocity vector and the total energy per unit volume, respectively, τ_{ij} is the shear stress and q is the heat flux. The convective terms were discretized with the second-order Roe upwind scheme, and the viscous terms were discretized with the second-order central differencing scheme. All cases were run with Menter's $k-\omega$ SST turbulence model [33,34].

Following the work of [35], the jet strength is characterized by the momentum coefficient, C_μ , which is defined as follows

$$C_\mu = \frac{\dot{m} U_{jet}}{\frac{1}{2} \rho_\infty U_\infty^2 S_{ref}} \quad (3)$$

where $\dot{m} = \rho_{jet} U_{jet} S_{jet}$ is the jet mass flow rate, U_{jet} and U_∞ are the jet velocity and the freestream velocity, respectively, S_{jet} is the jet area, S_{ref} is the reference area of the aircraft, and ρ_∞ and ρ_{jet} are the freestream density and the jet density, respectively.

2.2. Baseline Geometry and Computational Grid

As shown in Figure 1, the baseline geometry, with a length of L_0 , a width of W_0 and a height of H_0 , is a hypersonic aircraft. It is a typical waverider equipped with a lifting body, which can be divided into three main parts, with a length of L_1 , L_2 and L_3 , respectively. Additionally, L_4 is the length of the aircraft tail, designed for controlling the aircraft. The other geometric parameters are shown in the figure as well. For convenience, the horizontal tail was ignored, and the air inlet and the engine nozzle were blocked. It is believed that the above simplifications are reasonable due to the fact that only relative lift changes are important in this context. All cases were conducted at a freestream Mach number of 0.3 with the angles of attack ranging from 0° to 20° , resulting in a Reynolds number of 2.34×10^7 . The jet slots were arranged along the side edges of the lifting body. Each jet slot had a length of $0.2 L_0$ in the x direction and a width of $0.088 H_0$ in the y direction, with a blowing direction parallel to the z -axis.

An unstructured grid was generated around the aircraft geometry, extending to the far-field $25 L_0$ away from the body surface in the x direction, and $21 W_0$ away from the body surface in both the y and z directions, as shown in Figure 2. To obtain a better spatial resolution of the jets, the hexahedral grid was generated around the jet slots, and the grid near the jet region was refined as well. The blowing boundary was modelled with a subsonic velocity inlet in the simulations. All solid surfaces were treated as no-slip walls.

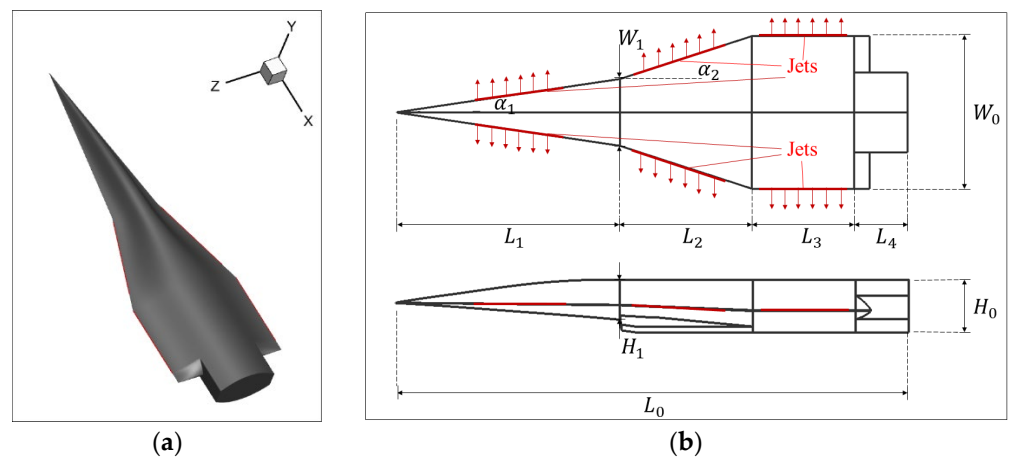
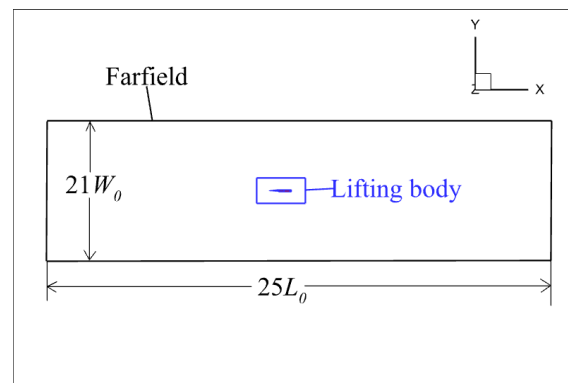
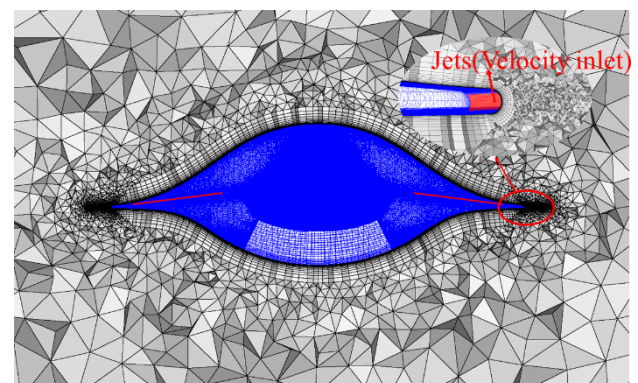
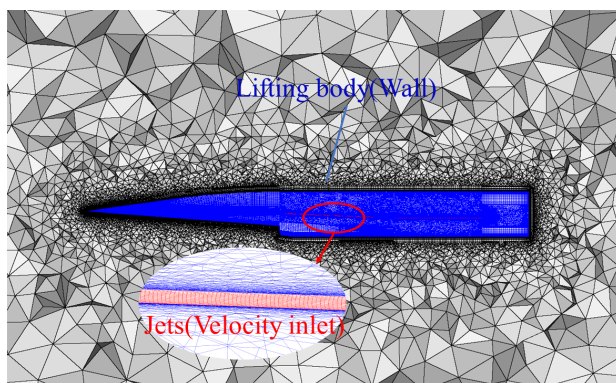


Figure 1. The baseline geometry. (a) Three-dimensional view; (b) Top and side views.



(a)



(b)

Figure 2. Computational grid. (a) Grid topology; (b) Surface and slice grid.

3. Validations

3.1. The BHV Model

In order to validate the numerical methods, a number of simulations were conducted to reproduce the results of an experiment carried out by Nelms and Thomas [36] in a wind tunnel. The BHV (Body, Horizontal tail and Vertical tail) model was designed to represent a hypersonic aircraft in their experiment. The configuration has a delta planform and an elliptical cross-section with two horizontal tails and two vertical tails as shown in Figure 3a. All of the geometric parameters are summarized in Table 1. The chosen Reynolds number was 8.2×10^6 based on the aircraft width, and the chosen Mach numbers were 0.65 and 1.1, respectively. An unstructured grid was generated around the BHV aircraft as shown in Figure 3b, and the total number of grid cells was about 5 million. Figure 4 shows

the comparison of the experimental data and the numerical results. The two data sets show a good agreement with both Mach numbers.

Table 1. Geometric parameters of BHV model.

Geometric Parameters	Value
length L_{bhv}	0.5397 m
width W_{bhv}	0.3114 m
area S_{bhv}	5.675 m ²

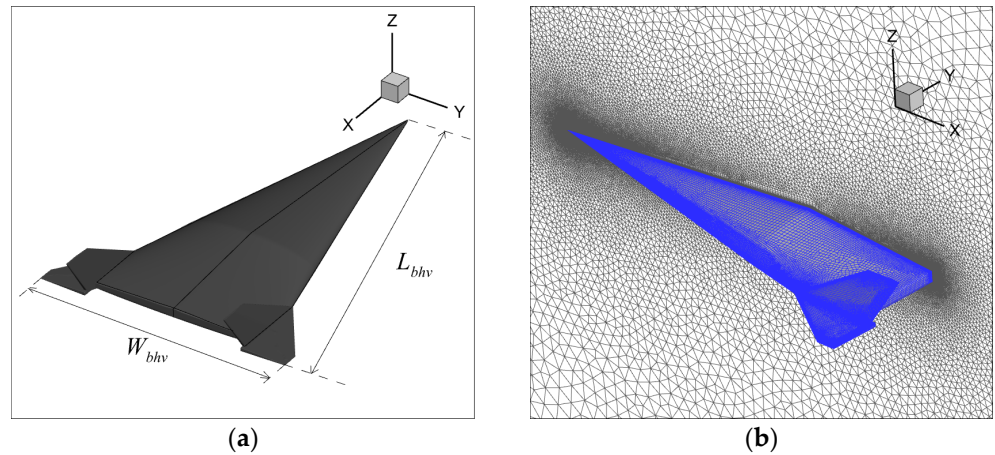


Figure 3. The experimental model and the computational grid. (a) BHV model; (b) Surface and slice grids.

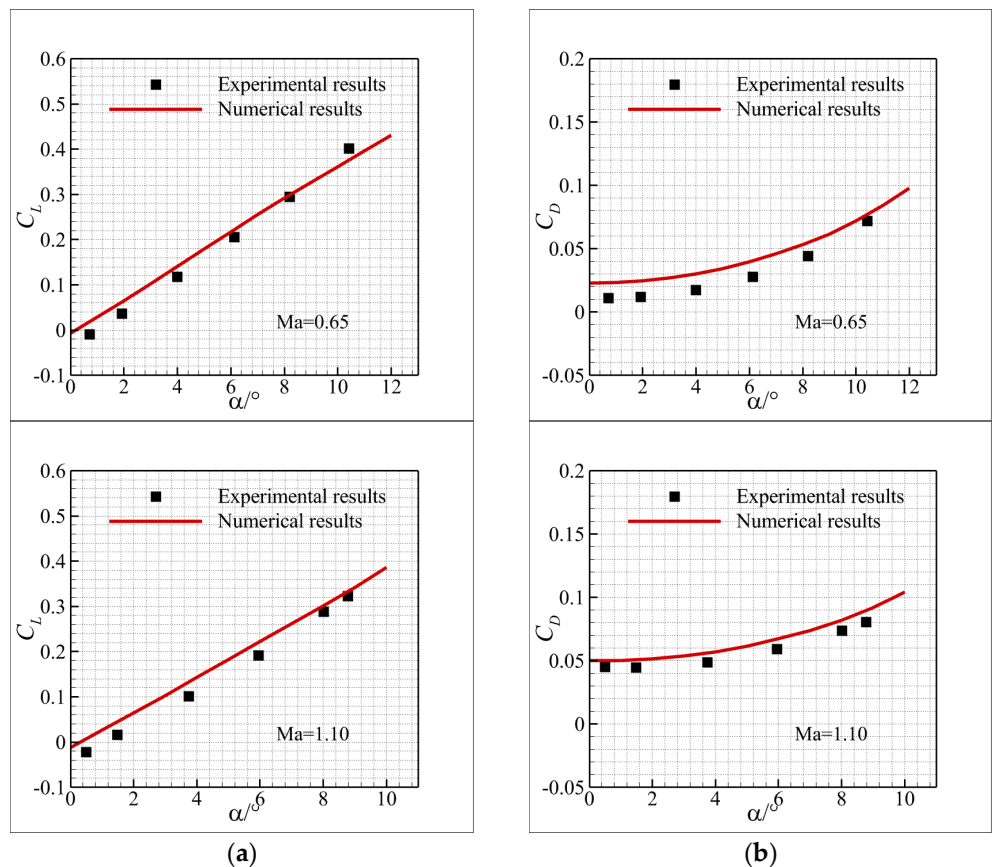


Figure 4. Comparison of the experimental and numerical results at $Ma = 0.65, 1.1$ and $Re = 8.2 \times 10^6$. (a) Lift coefficient; (b) Drag coefficient.

3.2. The Jet Modelling

To validate the accuracy of the jet modelling, an experiment carried out by Boeije et al. [37] was reproduced by numerical simulations in this section. Their experimental model had a NACA0018 airfoil profile, a chord of 0.165 m and a jet width of 0.001 m, located at the 90% chord line on the lower surface. The freestream velocity, U_∞ , was 58 m/s, the Reynolds number was 6.6×10^5 and the momentum coefficient, C_{μ} , was 0.012. In their experiment, two pressure ports were used to measure the pressure coefficient distributions along the upper and lower surfaces, respectively. Additionally, they had evaluated the changes in the lift with and without the microjets, while the lift coefficients were obtained numerically in the same condition as that in the experiment by using a software package, ANSYS CFX 11.0. As shown in Figure 5, the pressure coefficient distributions by numerical simulations agree well with the experimental data at both angles of attack. Figure 6 gives the comparison of the lift coefficients between the present and reference results. The two data sets also show a good agreement. As a result, the accuracy of the current numerical method is sufficient for this study.

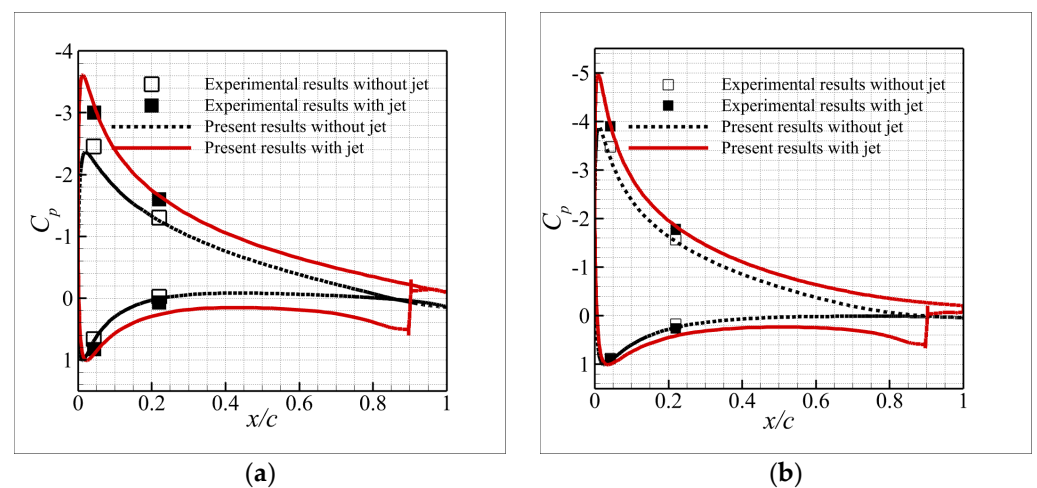


Figure 5. Comparison of the pressure coefficient distributions by the experimental and present results. (a) $\alpha = 8^\circ$; (b) $\alpha = 12^\circ$.

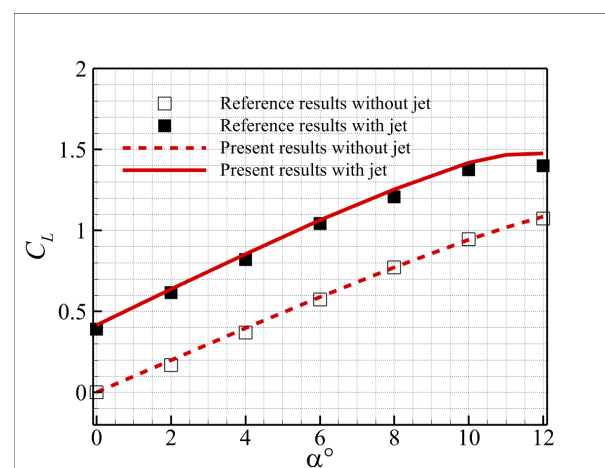


Figure 6. Comparison of the lift coefficients by the present and reference results [37].

3.3. Grid Convergence Study

A grid convergence study was carried out to ensure a grid independence result. Three grids with different densities were generated for the study as shown in Table 2 and Figure 7. The finer grid was generated through refining the grid points along both the streamwise

and spanwise directions, as well as increasing the number of surface grid cells near the jets. The average y^+ of the first cell normal to the body surface was kept below one for an appropriate near-wall turbulence modelling, as shown in Table 2. The simulations were conducted for four different jet momentum coefficients at a Mach number of 0.3 and an angle of attack of 10° . Figure 8 gives the comparison of the lift and drag coefficients between the three grids. It can be seen that the lateral blowing causes an increase in both the lift and drag coefficients. The results on different grids are very close to each other, and only minor differences can be noticed for the coarse grid. Thus, the following study will proceed with the medium grid by considering a trade-off between the numerical accuracy and the computational costs. By using a high-performance computer with a total of eight Intel E5-2620 v4 CPUs, the time cost of each run was about 8 h.

Table 2. Grids for the grid convergence study.

Grid Type	Number of Grid Points	Number of Cells for Each Jet	Average y^+
coarse grid	9.7 million	501×7	0.57
medium grid	21 million	801×13	0.52
fine grid	38 million	1201×17	0.44

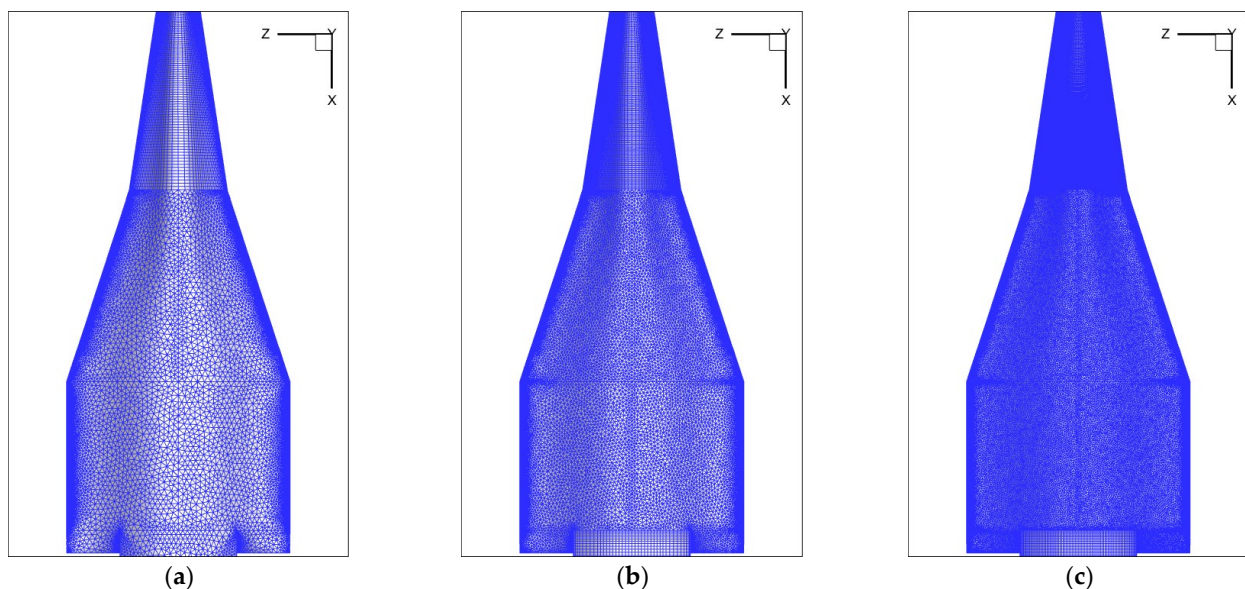


Figure 7. Grids for the grid convergence study. (a) Coarse grid; (b) Medium grid; (c) Fine grid.

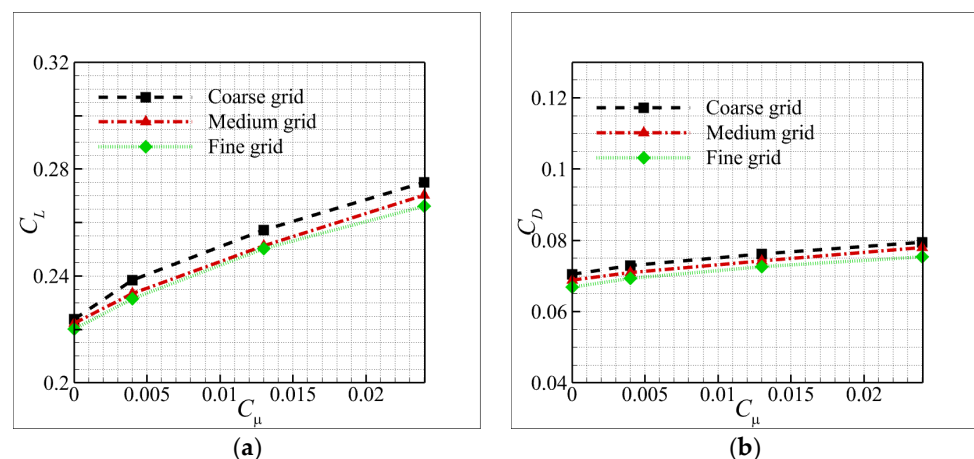


Figure 8. The results of the grid convergence study at $\alpha = 10^\circ$. (a) Lift coefficient; (b) Drag coefficient.

4. Results and Discussion

4.1. Effect of Jet Location

The effect of the jet location on lift augmentation was first studied by designing five jet configurations, as shown in Figure 9. The jet slots were arranged along the side edges of the front part, the middle part and the rear part of the lifting body, respectively, as well as their combinations. The corresponding jet regions in the x direction are $(0.15 L_0, 0.35 L_0)$, $(0.45 L_0, 0.65 L_0)$ and $(0.7 L_0, 0.9 L_0)$, respectively. Each slot has a length of $0.2 L_0$ in the x direction and a width of $0.088 H_0$ in the y direction. All cases were chosen with the same jet momentum coefficient, C_{μ} , of 0.013 and the same jet direction; parallel to the z -axis.

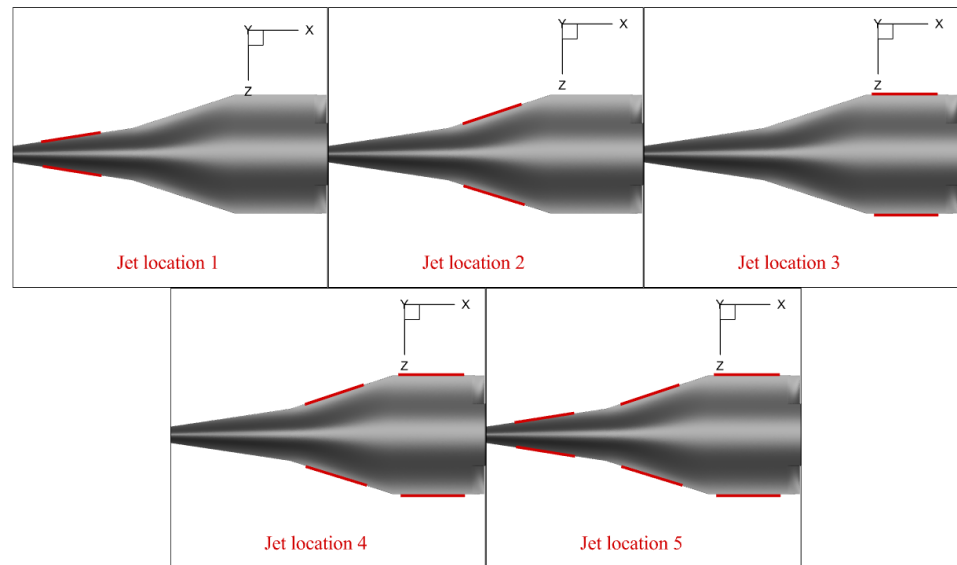


Figure 9. Lifting bodies with different jet locations.

Figure 10 presents the comparison of the lift augmentation by different jet configurations at the angles of attack ranging from 10° to 20° . In the figure, “Baseline” represents the results of the clean body. It is clear that the “Jet location 4” configuration achieves the maximum lift augmentation among the five cases. In addition, the other configurations produce promising results as well, except for the “Jet location 1” configuration, which produces a relatively small lift augmentation.

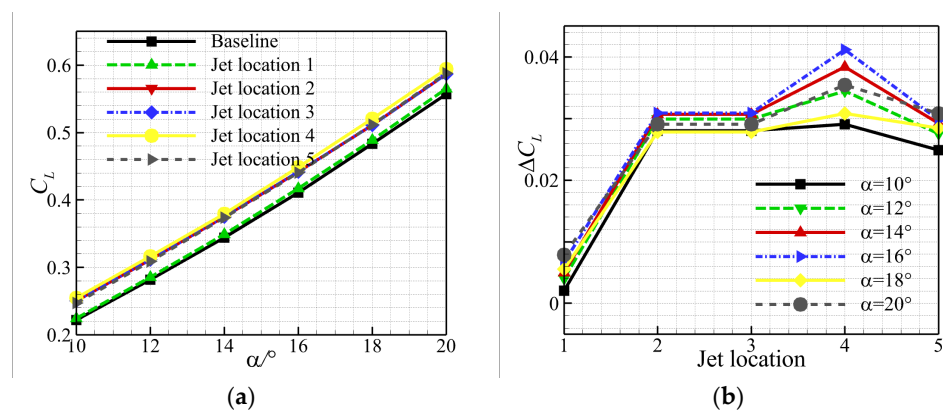


Figure 10. Changes in lift by the lateral jets at different jet locations. (a) Lift coefficient; (b) Lift coefficient augmentation.

Figure 11 gives the comparison of the pressure coefficient distributions at the chosen five cross sections located at $x/L_0 = 0.25, 0.5, 0.6, 0.75$ and 0.8 , respectively. It can be seen that the lateral blowing causes a high suction peak on the upper surface, while only minor

changes in the pressure can be seen on the lower surface. By further examining the contours of the surface pressure coefficients, shown in Figure 12, it is clear that the pressure on the upper surface decreases due to a lateral blowing, resulting in an increase in the overall lift. The only exception is blowing on the front part of the lifting body, corresponding to the “Jet location 1” configuration. Although the “Jet location 1” configuration produces an increase in the local lift on the front part of the body, it causes a drop of suction peak on the middle and rear parts of the body, resulting in a decrease in the overall lift.

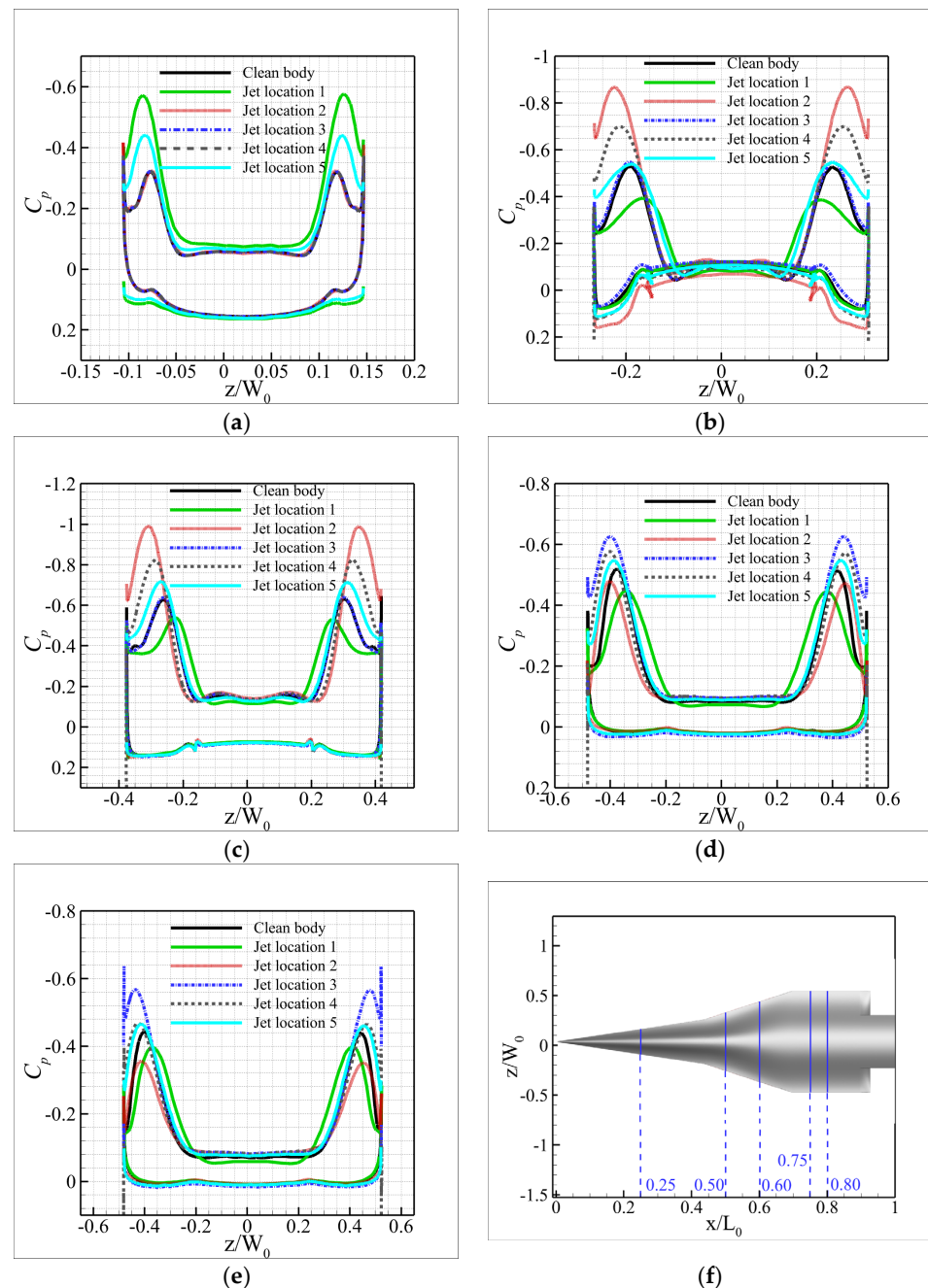


Figure 11. Comparison of the pressure coefficient distributions at the chosen cross-sections for different jet locations at $\alpha = 10^\circ$. (a) $x/L_0 = 0.25$; (b) $x/L_0 = 0.5$; (c) $x/L_0 = 0.6$; (d) $x/L_0 = 0.75$; (e) $x/L_0 = 0.8$; (f) Illustration of the cross-sections.

The lift rise achieved by the lateral jets can be associated with the leading-edge vortices, as shown in Figures 13 and 14. For each configuration, two counter-rotating vortex pairs can be clearly observed, inducing a low pressure on the upper surface of the lifting body.

Due to a well-designed lateral blowing, such as that of the “Jet location 4” configuration, the strength of the leading-edge vortices has been reinforced, resulting in an increase in the vortex lift. However, blowing on the front part of the lifting body, such as that in the “Jet location 1” configuration, is similar to the effect of a canard wing, causing an unfavorable interference downstream. For this unfavorable blowing, the leading-edge vortices shedding from the front part of the body merge with the downstream vortices, causing them to move upwards. As a result, the suction peaks on the middle and rear parts of the body decrease and so does the overall lift.

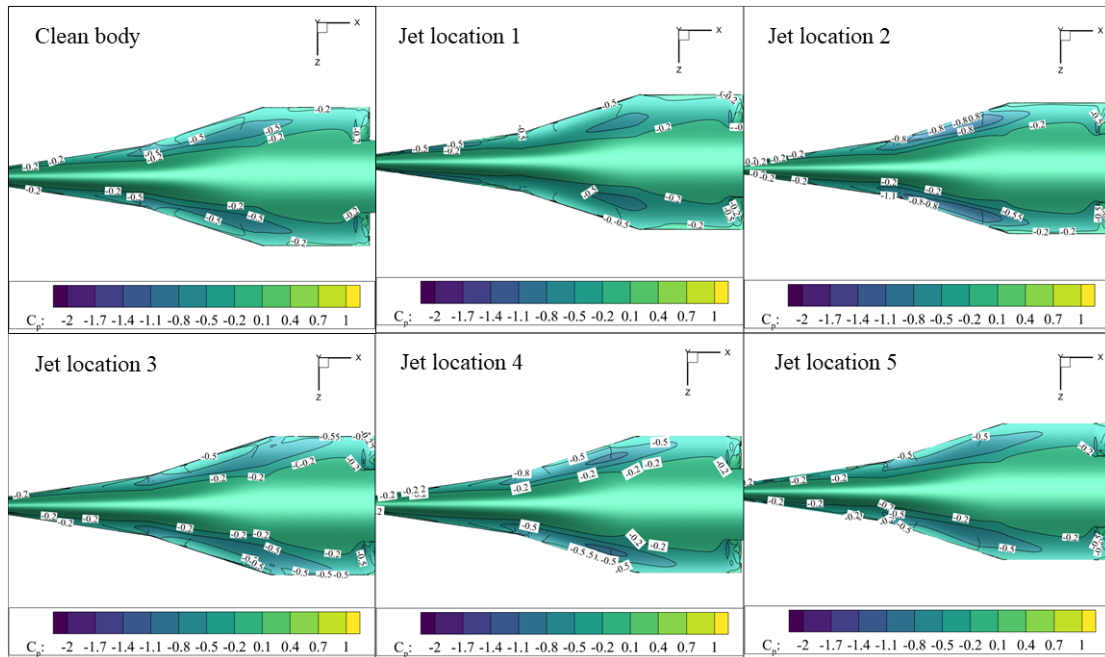


Figure 12. Comparison of the pressure coefficient contours on the upper surfaces for different jet locations at $\alpha = 10^\circ$.

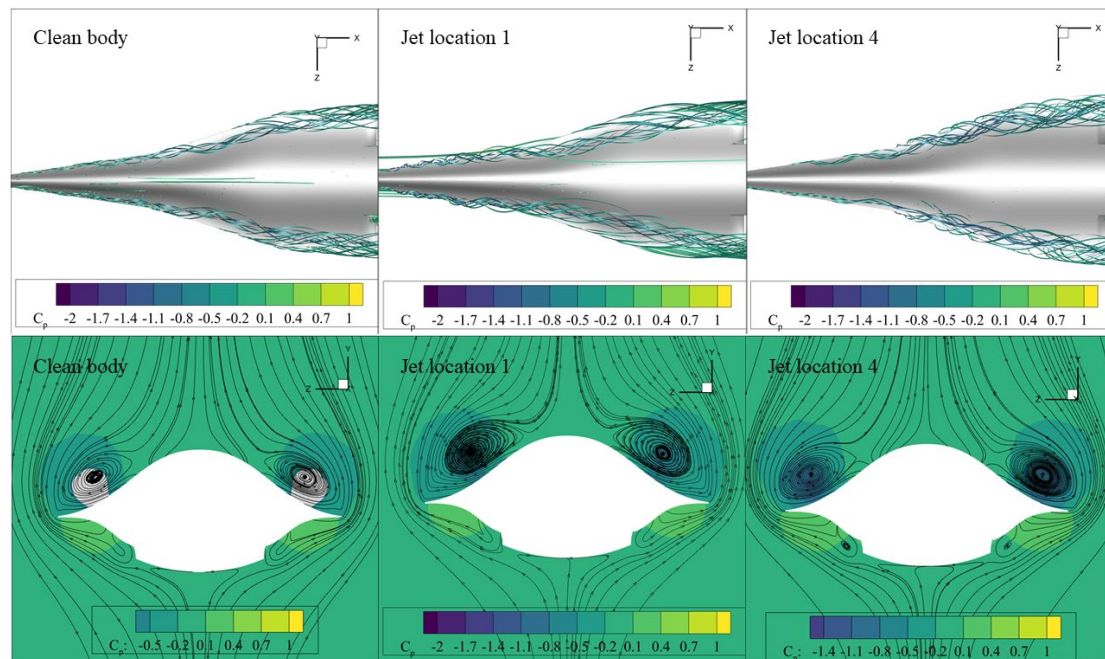


Figure 13. Comparison of the streamlines for different blowing directions at $\alpha = 10^\circ$, $x/L_0 = 0.6$.

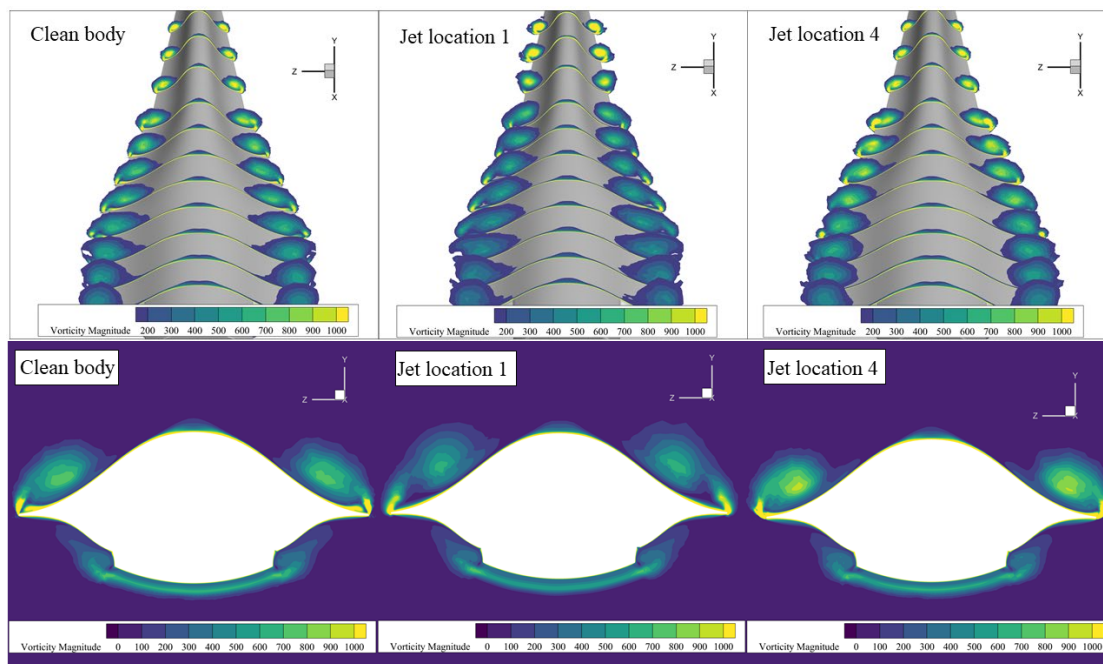


Figure 14. Comparison of the vorticity contours for different blowing directions at $\alpha = 10^\circ$.

As mentioned above, the flow mechanism associated with the lift rise is that a well-designed blowing reinforces the strength of the leading-edge vortices and induces more vortices shedding from the side edges, resulting in an increase in the vortex lift. This lift generation mechanism is analogous to that of adding long strake wings along the side edges of the aircraft, as shown in the study by Luckring [7].

4.2. Effect of Blowing Strength

The above study shows that the lateral jets can effectively increase the local lift on the middle and rear parts of the lifting body. In this section, further studies on the effect of blowing strength are presented by varying the jet momentum coefficient, C_{μ} . The flows were simulated at an angle of attack of 10° with the “Jet location 4” configuration as shown in Figure 9. The blowing direction was fixed parallel to the z-axis.

Figure 15 shows the changes in lift coefficient for different jet momentum coefficients, ranging from 0 to 0.045. As expected, it can be seen that the lift increases as the jet momentum coefficient increases. In addition, the changes in lift are relatively insensitive to the angle of attack. When $C_{\mu} = 0.045$, the peak relative change in lift coefficient is close to 0.09. By examining the pressure coefficient distributions and the pressure coefficient contours shown in Figures 16 and 17, respectively, it is clear that both the suction peak and the size of low-pressure area increase as the blowing strength increases, resulting in an increase in the overall lift. The effectiveness of increasing the jet momentum coefficient can be explained by the same flow mechanism as mentioned in the previous section. As shown in Figures 18 and 19, a stronger blowing induces stronger leading-edge vortices, resulting in a higher vortex lift.

Following the work of [38], the jet power consumption is determined by the mass flow and the total enthalpy as follows,

$$P_{jet} = \frac{\dot{m}c_p T_{01}}{\eta} \left((P_{01}/P_{00})^{\frac{\gamma-1}{\gamma}} - 1 \right) \quad (4)$$

where \dot{m} is the jet mass flow, c_p and γ are the air specific heat at constant pressure and the air specific heat ratio, respectively, T_{01} is the total temperature, P_{01} is the mass-averaged total pressure of the jet flow, P_{00} is the free-stream static pressure and $\eta = 1$ is the pump

efficiency. The power consumption can be nondimensionalized by the free-stream dynamic pressure, $\frac{1}{2}\rho_\infty U_\infty^2$, and velocity, U_∞ , as follows,

$$C_{power} = \frac{P_{jet}}{\frac{1}{2}\rho_\infty U_\infty^3 S_{ref}} \tag{5}$$

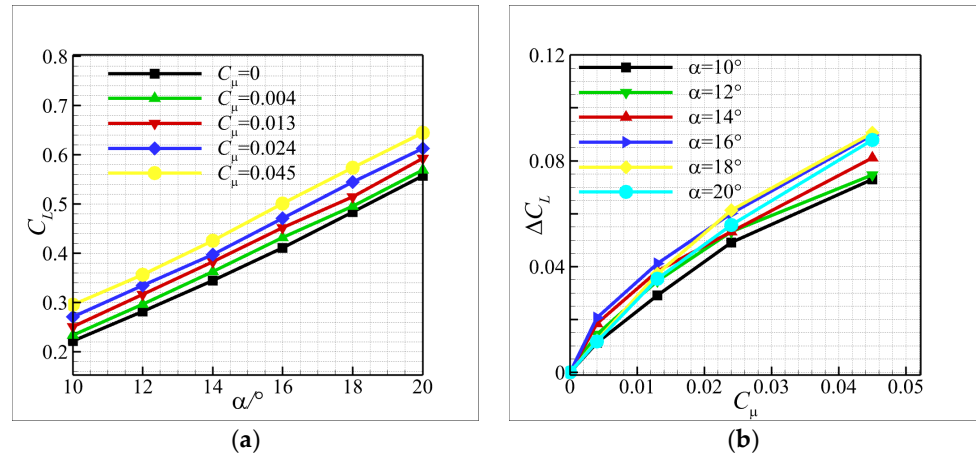


Figure 15. Changes in lift by the lateral jets with different jet momentum coefficients. (a) Lift coefficient; (b) Lift coefficient augmentation.

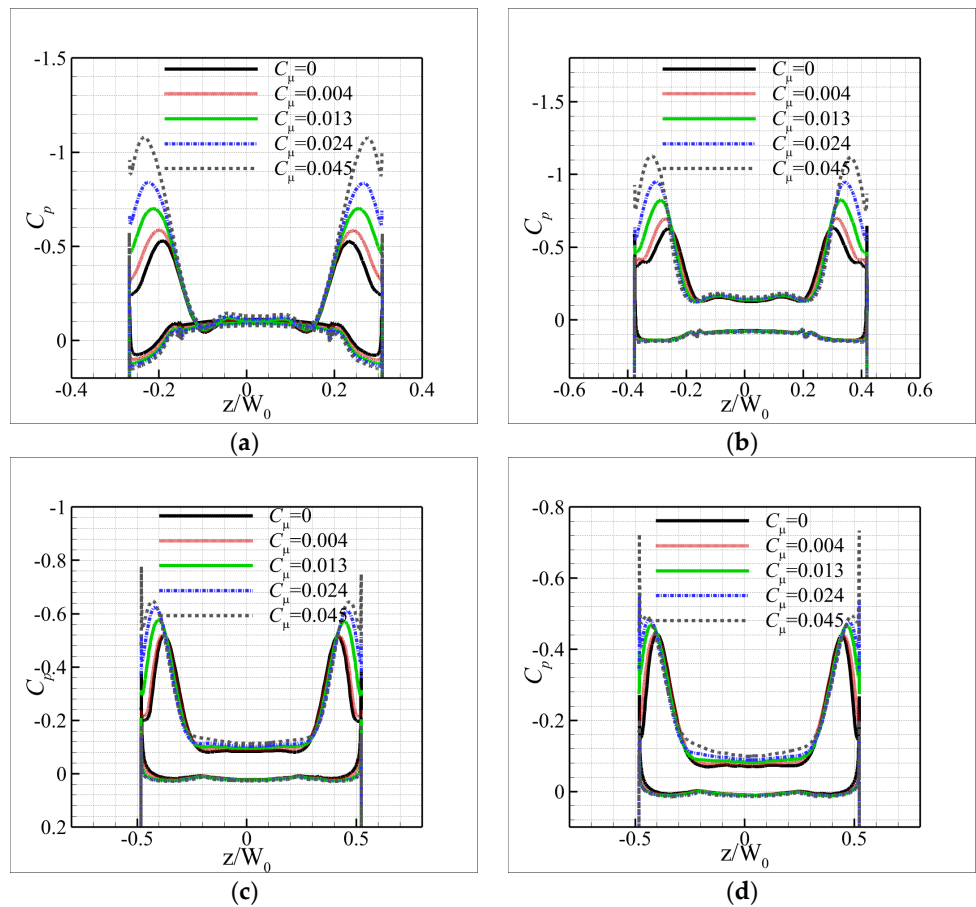


Figure 16. Comparison of the pressure coefficient distributions at the chosen cross-sections by the lateral jets with different jet momentum coefficients at $\alpha = 10^\circ$. (a) $x/L_0 = 0.5$; (b) $x/L_0 = 0.6$; (c) $x/L_0 = 0.75$; (d) $x/L_0 = 0.8$.

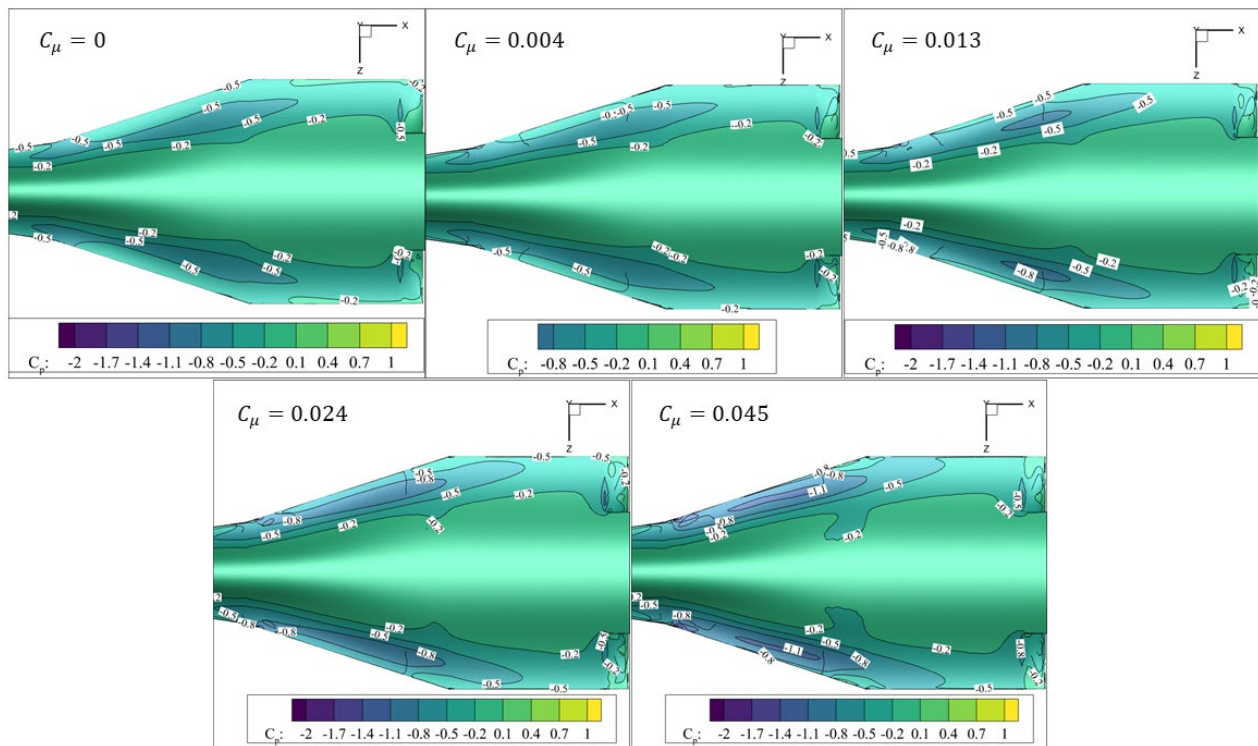


Figure 17. Comparison of the pressure coefficient contours on the upper surfaces for different jet momentum coefficients at $\alpha = 10^\circ$.

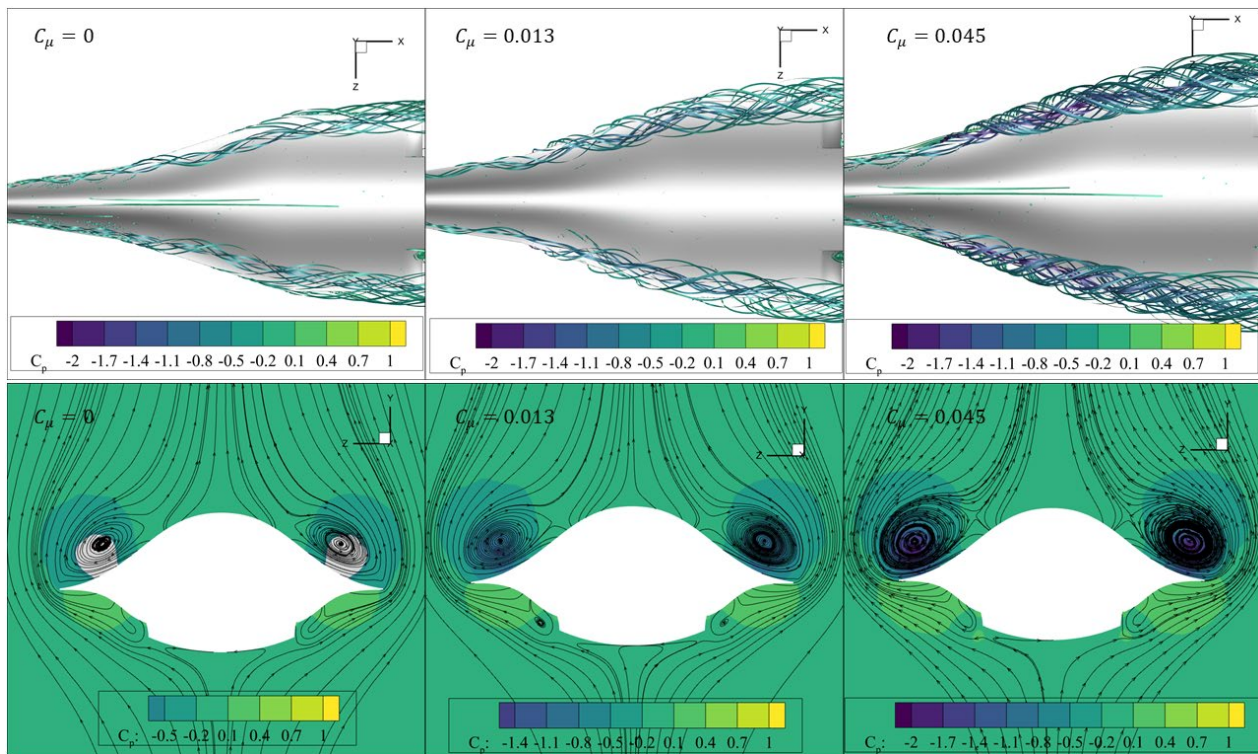


Figure 18. Comparison of the streamlines for different jet momentum coefficients at $\alpha = 10^\circ$.

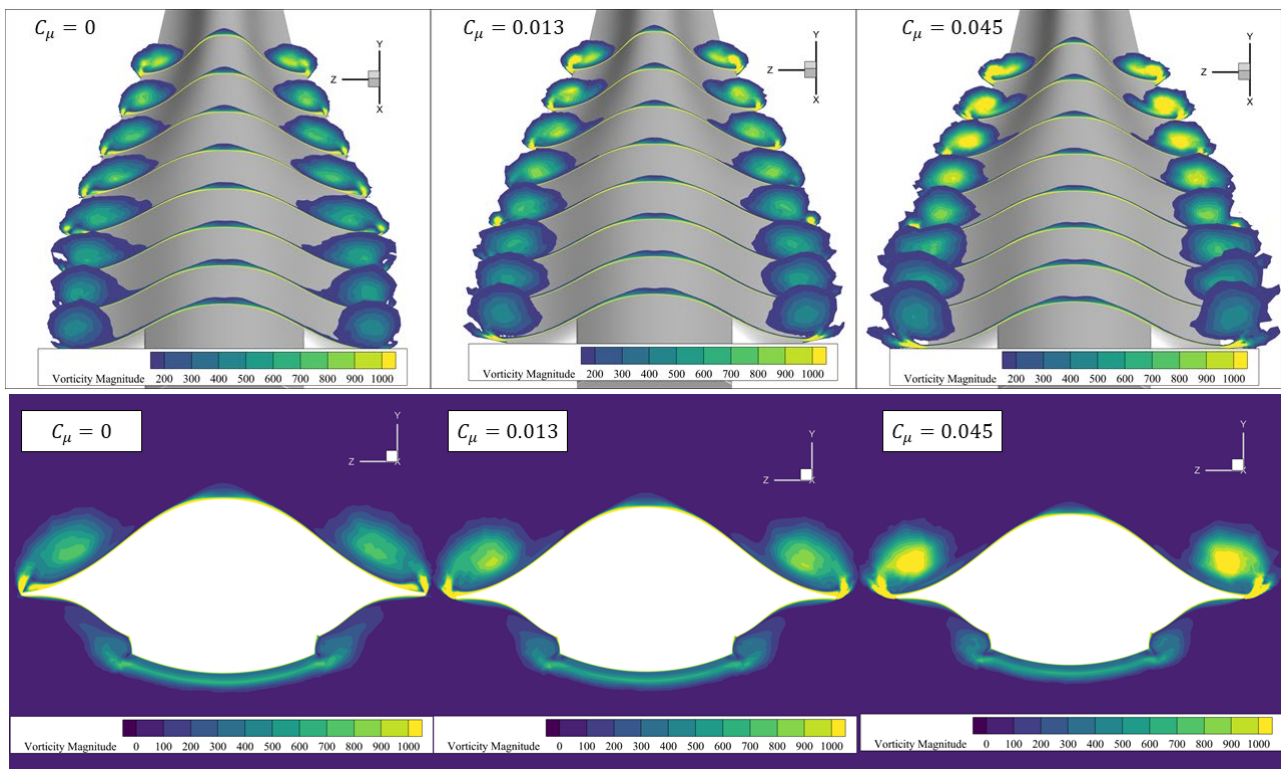


Figure 19. Comparison of the vorticity contours for different jet momentum coefficients at $\alpha = 10^\circ$, $x/L_0 = 0.6$.

By assuming that the drag is balanced by the thrust during the cruise flight, the thrust power consumption of the engines can be defined as $P_{thrust} = T \cdot U_\infty = D \cdot U_\infty$. Therefore, the power consumption ratio can be expressed as follows,

$$\varepsilon = \frac{P_{jet}}{P_{thrust} + P_{jet}} = \frac{P_{jet}}{D \cdot U_\infty + P_{jet}} = \frac{C_{power}}{C_D + C_{power}} \quad (6)$$

Table 3 gives several typical values of ε corresponding to the chosen jet momentum coefficients, C_μ . It can be seen that the jet power consumption accounts for a small percentage of the total power consumption.

Table 3. Jet power consumption ratios corresponding to the chosen jet momentum coefficients.

C_μ	ε
0.000	0.00%
0.013	1.14%
0.045	4.05%

4.3. Effect of Blowing Direction

In addition to the jet location and the blowing strength, the blowing direction is another key parameter for the control effectiveness of the lateral jets. As shown in Figure 20, the jet direction, θ_{jet} , is defined as the angle between the blowing direction and the z-axis. A positive value means pointing towards the upper surface of the lifting body, and a negative value means pointing towards the lower surface of the lifting body. Five jet configurations with the blowing directions of $\theta_{jet} = \pm 45^\circ$, $\pm 30^\circ$ and 0° were considered in this study. The baseline configuration was assumed to be $\theta_{jet} = 0^\circ$. According to the previous studies, the jet momentum coefficient was chosen as 0.013 and four jet slots were placed on the

middle and rear parts of the lifting body such as that in the “Jet location 4” configuration shown in Figure 9.

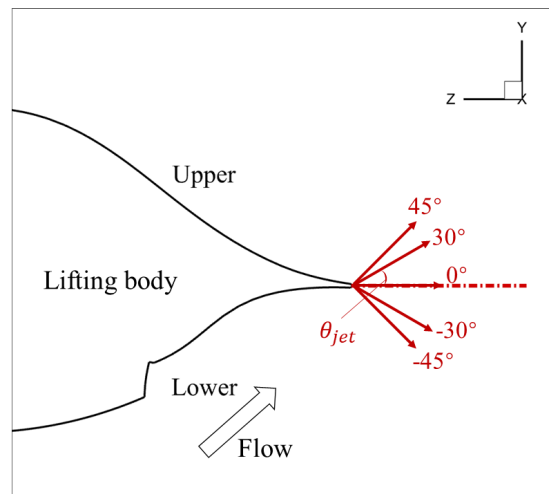


Figure 20. Definition of the blowing direction.

Figure 21 presents the lift changes for different blowing directions. It can be observed that a high lift rise is obtained when $\theta_{jet} = -45^\circ$ or $\theta_{jet} = -30^\circ$, whereas the lift augmentation decreases when $\theta_{jet} = 30^\circ$ or $\theta_{jet} = 45^\circ$. It indicates that blowing towards the lower surface has a better control effect than blowing towards the upper surface. The pressure coefficient distributions and the pressure coefficient contours shown in Figures 22 and 23, respectively, confirm the same observation. The suction peak in the case of $\theta_{jet} = -45^\circ$ is higher than that of $\theta_{jet} = 45^\circ$. In contrast to increasing the jet moment coefficient, changing the blowing direction causes minor changes in the strength of leading-edge vortices, as shown in Figures 24 and 25. However, blowing towards the upper surface moves the leading-edge vortices slightly upwards, causing a decrease in generating the vortex lift. This is similar to the unfavorable interference caused by the leading vortices shedding from the front part of the body, as discussed in the case of the “Jet location 1” configuration.

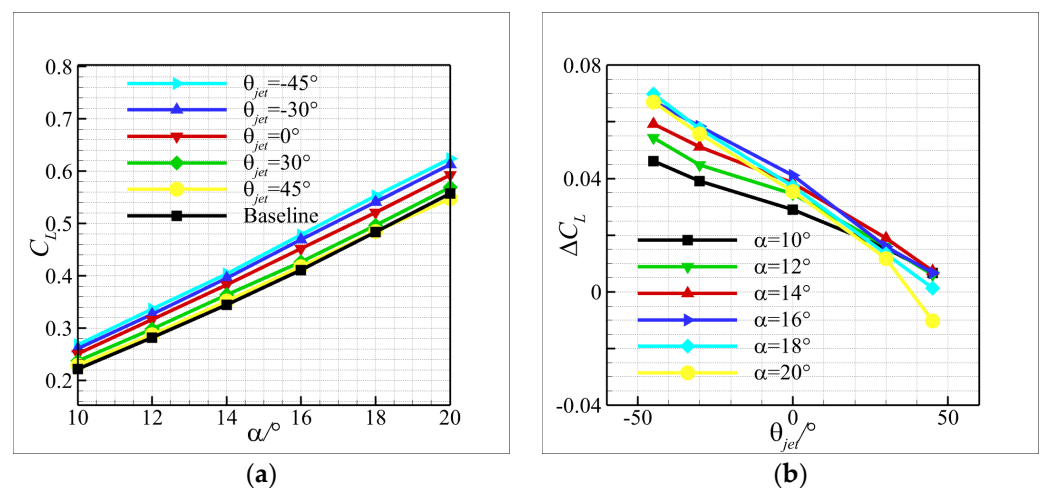


Figure 21. Changes in lift by the lateral jets with different blowing directions. (a) Lift coefficient; (b) Lift coefficient augmentation.

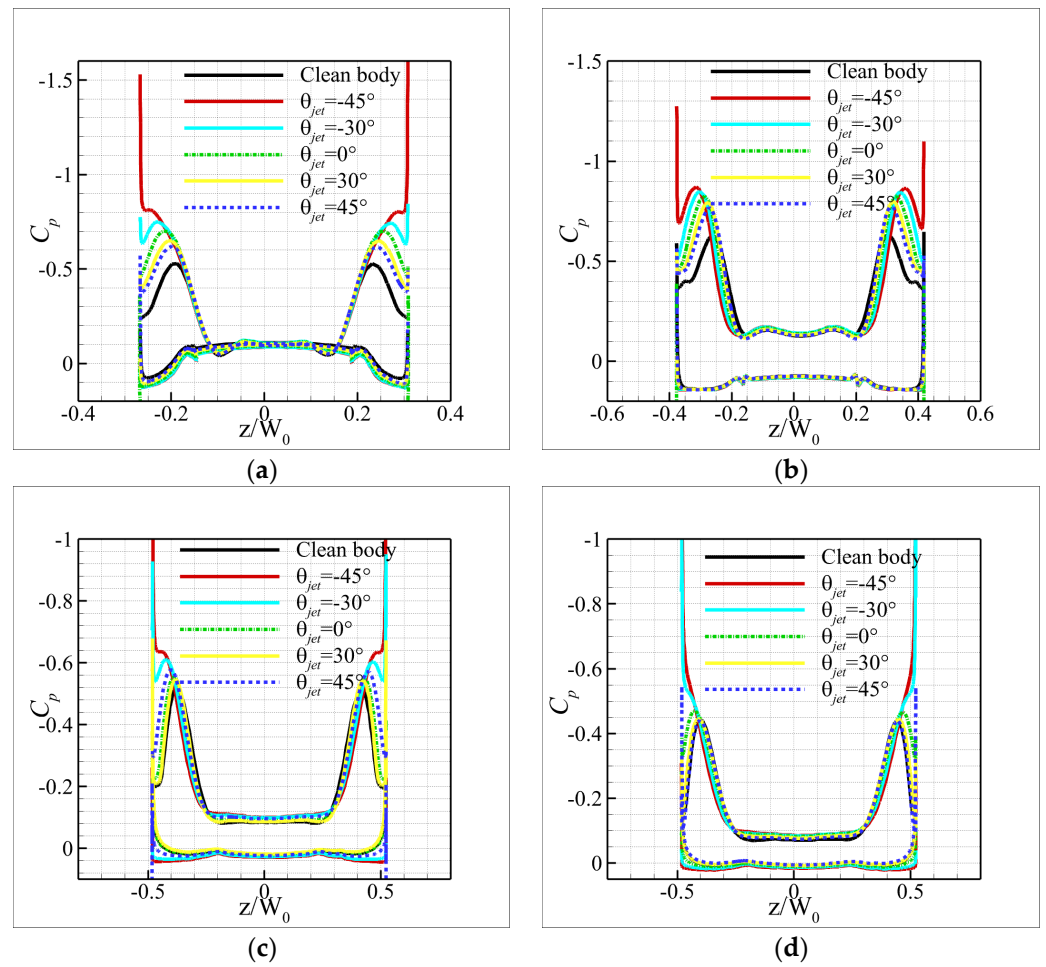


Figure 22. Comparison of the pressure coefficient distributions at the cross-sections for different blowing directions at $\alpha = 10^\circ$. (a) $x/L_0 = 0.5$; (b) $x/L_0 = 0.6$; (c) $x/L_0 = 0.75$; (d) $x/L_0 = 0.8$.

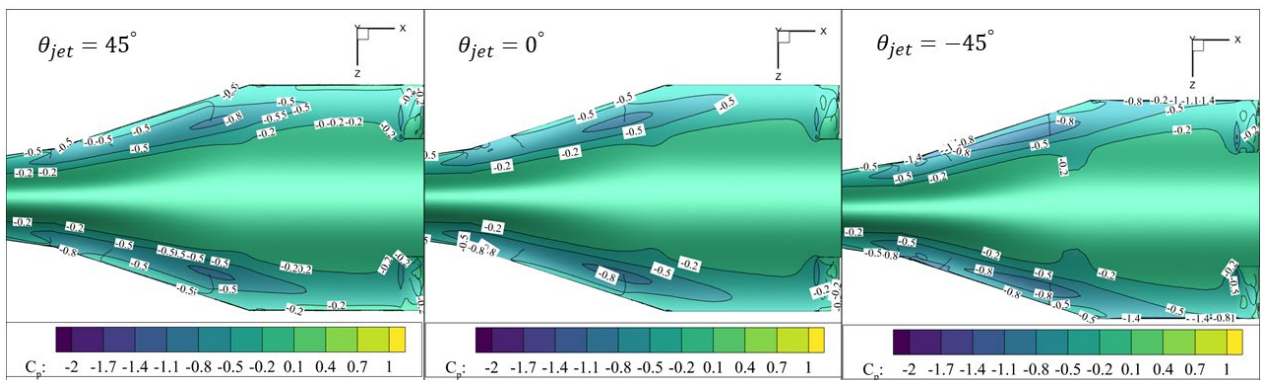


Figure 23. Comparison of the pressure coefficient distributions on the upper surfaces for different blowing directions at $\alpha = 10^\circ$.

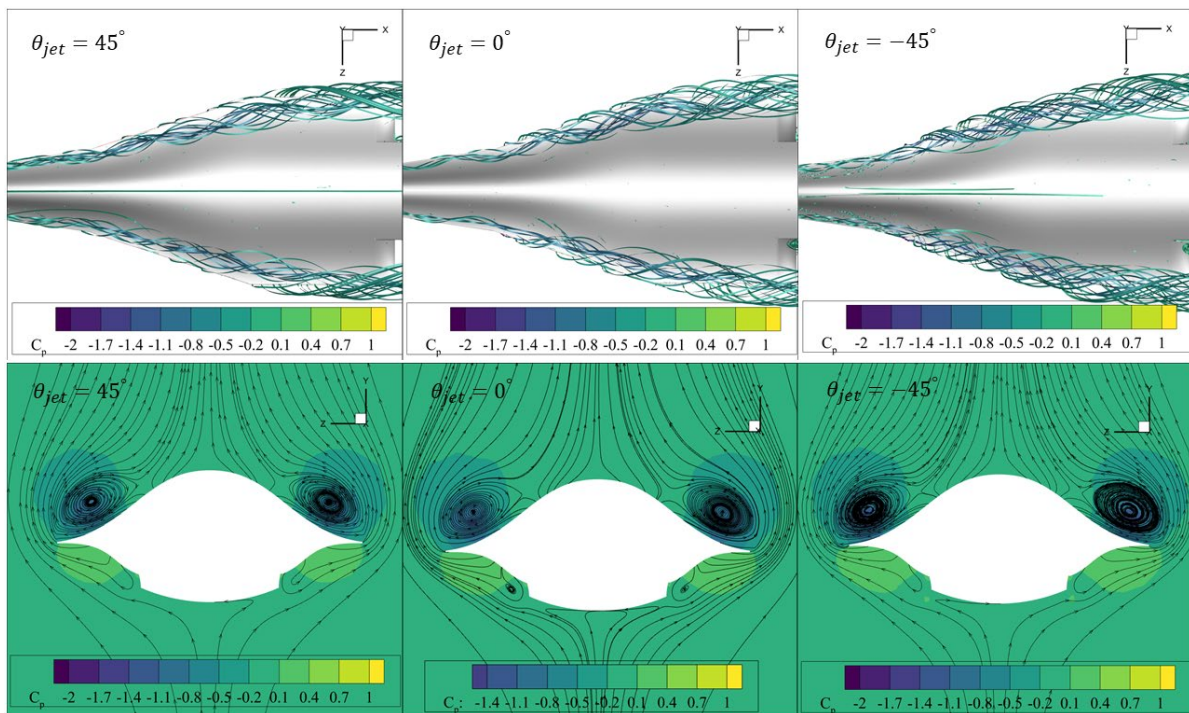


Figure 24. Comparison of the streamlines for different blowing directions at $\alpha = 10^\circ$, $x/L_0 = 0.6$.

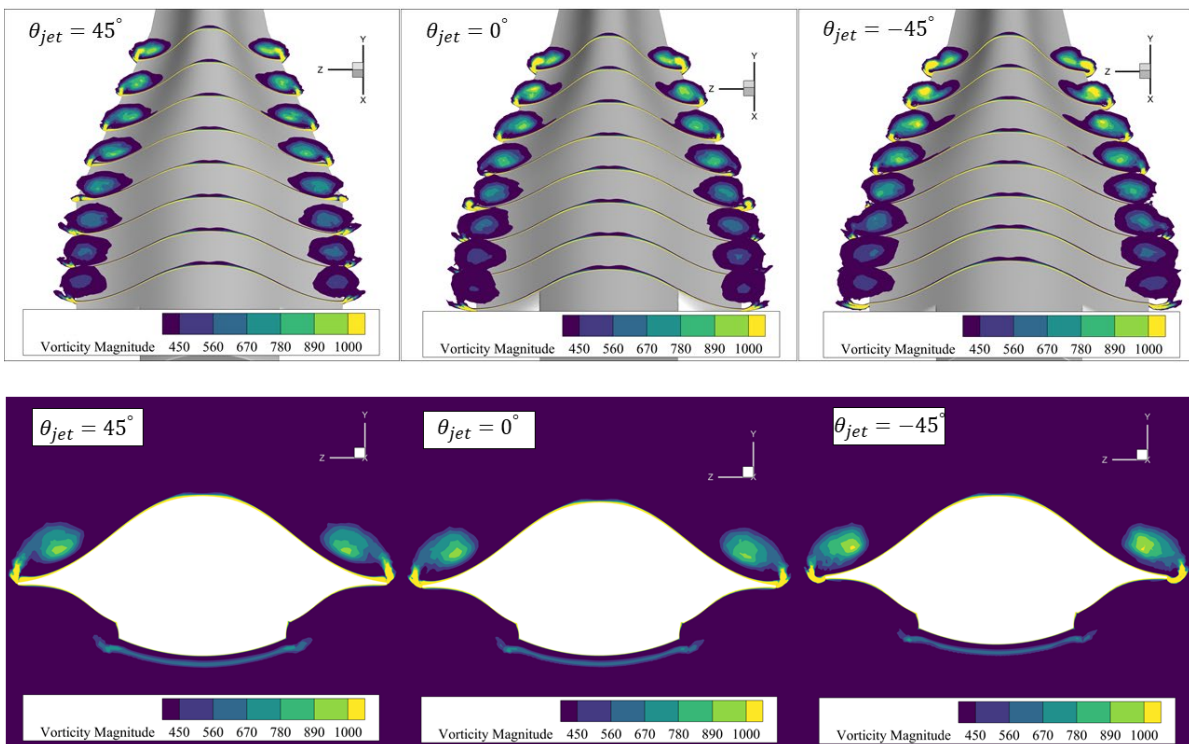


Figure 25. Comparison of the vorticity contours for different blowing directions at $\alpha = 10^\circ$, $x/L_0 = 0.6$.

Therefore, not only the strength of the leading-edge vortices but also the vortices' locations relative to the body's surface play important roles in producing the vortex lift for a given low aspect ratio lifting body. Note that a well-designed lateral blowing should be able to enhance the strength of the vortices and move the vortices' locations closer to the body's surface.

5. Conclusions

The effects of the lateral jets and the corresponding jet parameters on the low-speed performance of a hypersonic aircraft have been investigated numerically. It has been confirmed that the lateral jets can produce a significant increase in the overall lift. Three key jet parameters, including the jet location, the blowing direction and the blowing strength, have been investigated. The results show that the lift augmentation strongly depends on the jet parameters. It has been found that the “Jet location 4” configuration, in which four jet slots are placed on the middle and rear parts of the aircraft, achieves the maximum lift augmentation among the five chosen configurations. In contrast, blowing on the leading edge of the front part gives a relatively small contribution to lift improvement. Then, it was found that the lift augmentation increases as the blowing strength increases, due to the fact that a stronger blowing induces stronger leading-edge vortices. Additionally, blowing in the directions towards the lower surface, namely $\theta_{jet} = -45^\circ$ or $\theta_{jet} = -30^\circ$, achieves more lift augmentation than blowing in other directions, namely $\theta_{jet} = 0^\circ$, $\theta_{jet} = 30^\circ$ or $\theta_{jet} = 45^\circ$. In particular, the jet with $\theta_{jet} = -45^\circ$ produces the maximum lift augmentation among the chosen configurations. Furthermore, it is found that both the strength and the locations of the leading-edge vortices play important roles in producing the vortex lift. Note that a well-designed lateral blowing should be able to enhance the strength of the vortices and move the vortices’ locations closer to the body’s surface.

Author Contributions: Conceptualization, F.D., J.L., G.L., Y.D., Q.X. and F.Z.; software, J.L., G.L., Y.D., Q.X. and F.Z.; validation, H.W.; formal analysis, H.W. and F.D.; investigation, H.W. and F.D.; resources, F.D.; data curation, H.W.; writing—original draft preparation, H.W. and F.D.; writing—review and editing, F.D.; visualization, H.W.; supervision, F.D.; project administration, F.D.; funding acquisition, F.D. All authors have read and agreed to the published version of the manuscript.

Funding: This research was supported by the National Natural Science Foundation of China (No. 11672132) and a project funded by the Priority Academic Program Development of Jiangsu Higher Education Institutions.

Institutional Review Board Statement: Not applicable.

Informed Consent Statement: Not applicable.

Data Availability Statement: Some or all data, models, or code that support the findings of this study are available from the corresponding author upon reasonable request.

Conflicts of Interest: The authors declare no conflict of interest.

References

1. Sobieczky, H.; Dougherty, F.C.; Jones, K. Hypersonic Waverider Design from given Shock Waves. In Proceedings of the International Hypersonic Waverider Symposium, College Park, MD, USA, 17–19 October 1990.
2. Rasmussen, M.L. Waverider Configurations Derived from Inclined Circular and Elliptic Cones. *J. Spacecr. Rocket.* **1980**, *17*, 537–545. [[CrossRef](#)]
3. Smith, A.M.O. High-Lift Aerodynamics. *J. Aircr.* **1975**, *12*, 501–530. [[CrossRef](#)]
4. Staelens, Y.D.; Blackwelder, R.F.; Page, M.A. Computer Simulation of Landing, Takeoff and Go-around of a Blended-Wing-Body Airplane with Belly-Flaps. In Proceedings of the 46th AIAA Aerospace Sciences Meeting and Exhibit, Reno, NV, USA, 7–10 January 2008.
5. Hummel, D.; Oelker, H. Low-Speed Characteristics for the Wing-Canard Configuration of the International Vortex Flow Experiment. *J. Aircr.* **1994**, *31*, 868–878. [[CrossRef](#)]
6. Tu, E.L. Effect of Canard Position on the Longitudinal Aerodynamic Characteristics of a Close-Coupled Canard-Wing-Body Configuration. In Proceedings of the Astrodynamics Conference, Hilton Head Island, SC, USA, 10–12 August 1992.
7. Luckring, J.M. Aerodynamics of Strake-Wing Interactions. *J. Aircr.* **1979**, *16*, 756–762. [[CrossRef](#)]
8. Tian, C.; Li, N.; Gong, G.; Su, Z. A Parameterized Geometry Design Method for Inward Turning Inlet Compatible Waverider. *Chin. J. Aeronaut.* **2013**, *26*, 1135–1146. [[CrossRef](#)]
9. Greenblatt, D.; Wagnanski, I.J. Control of Flow Separation by Periodic Excitation. *Prog. Aerosp. Sci.* **2000**, *36*, 487–545. [[CrossRef](#)]
10. Zhang, H.; Chen, S.; Meng, Q.; Wang, S. Flow Separation Control Using Unsteady Pulsed Suction through Endwall Bleeding Holes in a Highly Loaded Compressor Cascade. *Aerosp. Sci. Technol.* **2018**, *72*, 455–464. [[CrossRef](#)]
11. Li, Y.; Qin, N. Gust Load Alleviation by Normal Microjet. *Aerosp. Sci. Technol.* **2021**, *117*, 106919. [[CrossRef](#)]

12. Chan, D.T.; Jones, G.S.; Milholen, W.E.; Goodli, S.L. Transonic Drag Reduction through Trailing-Edge Blowing on the FAST-MAC Circulation Control Model. In Proceedings of the 35th AIAA Applied Aerodynamics Conference, Denver, CO, USA, 5–9 June 2017.
13. Amitay, M.; Glezer, A. Role of Actuation Frequency in Controlled Flow Reattachment over a Stalled Airfoil. *AIAA J.* **2002**, *40*, 209–216. [[CrossRef](#)]
14. Srivastava, B. CFD Analysis and Validation of Lateral Jet Control of a Missile. In Proceedings of the 34th Aerospace Sciences Meeting and Exhibit, Reno, NV, USA, 15–18 January 1996.
15. Srivastava, B. Computational Analysis and Validation for Lateral Jet Controlled Missiles. *J. Spacecr. Rocket.* **1997**, *34*, 584–592. [[CrossRef](#)]
16. Chamberlain, R.; McClure, D.; Dang, A. CFD Analysis of Lateral Jet Interaction Phenomena for the Thaad Interceptor. In Proceedings of the 38th Aerospace Sciences Meeting and Exhibit, Reno, NV, USA, 10–13 January 2000.
17. Jie, T.; Gong, M.; Sun, X.; Chen, Z.; Liu, F. Numerical Study on Aerodynamic Heating of a Lateral Jet Controlled Rocket. In Proceedings of the AIAA AVIATION 2022 Forum, Chicago, IL & Virtual, USA, 27 June–1 July 2022.
18. Zhu, L.; Li, Y.; Gong, L.; Chen, X.; Xu, J. Coupled Investigation on Drag Reduction and Thermal Protection Mechanism Induced by a Novel Combinational Spike and Multi-Jet Strategy in Hypersonic Flows. *Int. J. Heat Mass Transf.* **2019**, *131*, 944–964. [[CrossRef](#)]
19. Dong, H.; Liu, J.; Chen, Z.; Zhang, F. Numerical Investigation of Lateral Jet with Supersonic Reacting Flow. *J. Spacecr. Rocket.* **2018**, *55*, 928–935. [[CrossRef](#)]
20. Jiang, Z.; Liu, Y.; Han, G.; Zhao, W. Experimental Demonstration of a New Concept of Drag Reduction and Thermal Protection for Hypersonic Vehicles. *Acta Mech. Sin. Lixue Xuebao* **2009**, *25*, 417–419. [[CrossRef](#)]
21. Erickson, G.E.; Campbel, J.F. *Improvement of Maneuver Aerodynamics by Spanwise Blowing*; NASA-TP-1065; NASA: Washington, DC, USA, 1978.
22. Liu, P.Q.; Wen, R.Y.; Zhang, G.W. Effects of Canard Sweep and Canard-Span Wise Blowing Magnitude on Lift Increment. *J. Aircr.* **2006**, *43*, 1369–1371. [[CrossRef](#)]
23. Satran, D.R.; Gilbert, W.P.; Anglin, E.L. *Low-Speed Stability and Control Wind-Tunnel Investigation of Effects of Spanwise Blowing on Fighter Flight Characteristics at High Angles of Attack*; NASA-TP-2431; NASA: Washington, DC, USA, 1985.
24. Hong, J.S.; Roberts, L. A Computational Study on the Effects of Leading Edge Lateral Blowing on Delta Wing Aerodynamics. In Proceedings of the 13th Applied Aerodynamics Conference, San Diego, CA, USA, 19–22 June 1995.
25. Hong, J.S.; Çelik, Z.Z.; Roberts, L. Effects of Leading-Edge Lateral Blowing on Delta Wing Aerodynamics. *AIAA J.* **1996**, *34*, 2471–2478. [[CrossRef](#)]
26. Kamishita, M.; Aso, S.; Karashima, K.; Sato, K. Active Control of Aerodynamic Characteristics of Next-Generation SST Wing by Lateral Blowing. In Proceedings of the 38th Aerospace Sciences Meeting and Exhibit, Reno, NV, USA, 10–13 January 2000.
27. Kamishita, M.; ASO, S.; Kamishita, K.; Sato, K. A Study on Improvement of Aerodynamic Characteristics of the Next-Generation SST Wing by Lateral Blowing in Subsonic Flow. *J. Jpn. Soc. Aeronaut. Space Sci.* **2001**, *49*, 174–180. [[CrossRef](#)]
28. Aso, S.; Kamishita, M.; Karashima, K.; Sato, K. A Study on Active Flow Control for Next-Generation SST for Higher L/D. In Proceedings of the 32nd AIAA Fluid Dynamics Conference and Exhibit, St. Louis, MO, USA, 24–26 June 2002.
29. Tadakuma, K.; Aso, S.; Ishida, T.; Tani, Y.; Nakawatase, R. Lift Augmentation by Lateral Blowing for RLVs with Various Fuselage-Cross Sections. In Proceedings of the Collection of Technical Papers—3rd AIAA Flow Control Conference, San Francisco, CA, USA, 5–8 June 2006.
30. Muramatsu, S.; Okada, S.; Hiraoka, K. Numerical Analysis of Control of Leading-Edge Vortex on Delta Wing with Blowing. In Proceedings of the 23rd AIAA Applied Aerodynamics Conference, Toronto, ON, Canada, 6–9 June 2005.
31. Zhang, J.M.; Cai, J.; Cui, Y. Effect of Nozzle Shapes on Lateral Jets in Supersonic Crossflows. In Proceedings of the 47th AIAA Aerospace Sciences Meeting including the New Horizons Forum and Aerospace Exposition, Orlando, FL, USA, 5–8 January 2009.
32. Doolabi, M.H.; Sabour, S.A.T. An Experimental Study of Binary Lateral Jets on a Standard Model in Subsonic, Transonic, and Supersonic Cross-Flows. *Proc. Inst. Mech. Eng. Part G J. Aerosp. Eng.* **2019**, *233*, 3141–3152. [[CrossRef](#)]
33. Menter, F.R. Two-Equation Eddy-Viscosity Turbulence Models for Engineering Applications. *AIAA J.* **1994**, *32*, 1598–1605. [[CrossRef](#)]
34. Menter, F.R.; Kuntz, M.; Langtry, R. Ten Years of Industrial Experience with the SST Turbulence Model. *Heat Mass Transf.* **2003**, *4*, 625–632.
35. Brunner, M.S.; Blaylock, M.; Cooperman, A.M.; Van Dam, C.P. Comparison of CFD with Wind Tunnel Tests of Microjets for Active Aerodynamic Load Control. In Proceedings of the 50th AIAA Aerospace Sciences Meeting including the New Horizons Forum and Aerospace Exposition, Nashville, TN, USA, 9–12 January 2012.
36. Nelms, W.P.; Thomas, C.L. *Aerodynamic Characteristics of an All-Body Hypersonic Aircraft Configuration at Mach Numbers from 0.65 to 10.6*; NASA Technical Note D-6577; NASA: Washington, DC, USA, 1971.
37. Boeije, C.S.; De Vries, H.; Cleine, I.; Van Emden, E.; Zwart, G.G.M.; Stobbe, H.; Hirschberg, A.; Hoeijmakers, H.W.M. Fluidic Load Control for Wind Turbine Blades. In Proceedings of the 47th AIAA Aerospace Sciences Meeting including the New Horizons Forum and Aerospace Exposition, Orlando, FL, USA, 5–8 January 2009.
38. Lefebvre, A.; Dano, B.; Bartow, W.B.; Difronzo, M.; Zha, G.C. Performance and Energy Expenditure of Coflow Jet Airfoil with Variation of Mach Number. *J. Aircr.* **2016**, *53*, 1757–1767. [[CrossRef](#)]